Slope stability analysis considering the strength anisotropy of c-φ soil

Yi He
Ministry of Education, Southwest Jiaotong University
Zhi Li
Southwest Jiaotong University
Wenfa Wang
Southwest Jiaotong University
Ran Yuan (yuanran@swjtu.edu.cn)
Ministry of Education, Southwest Jiaotong University
Xiaoyan Zhao
Southwest Jiaotong University
Nikolaos Nikitas
University of Leeds

Article

Keywords: Slope stability, Soil anisotropy, Finite element (FE) analysis, Stability, Safety factor, Soil constitutive laws

Posted Date: June 1st, 2022

DOI: https://doi.org/10.21203/rs.3.rs-1661050/v1

Title Page

Slope stability analysis considering the strength anisotropy of *c*-*φ* soil

Dr. Yi He
Key Laboratory of High-speed Railway Engineering, Ministry of Education, Southwest Jiaotong University, Chengdu 610031, China
Faculty of Geosciences and Environmental Engineering, Southwest Jiaotong University, Chengdu 611756, China
Email: heyi@swjtu.edu.cn

Zhi Li
Faculty of Geosciences and Environmental Engineering, Southwest Jiaotong University, Chengdu 611756, China
Email: zhili@my.swjtu.edu.cn

Wenfa Wang
Faculty of Geosciences and Environmental Engineering, Southwest Jiaotong University, Chengdu 611756, China
Email: alpha2324@my.swjtu.edu.cn

Dr. Ran Yuan*
Key Laboratory of High-speed Railway Engineering, Ministry of Education, Southwest Jiaotong University, Chengdu 610031, China
Key Laboratory of Transportation Tunnel Engineering, Southwest Jiaotong University, Chengdu 610031, China
Email: yuanran@swjtu.edu.cn

Dr. Xiaoyan Zhao
Faculty of Geosciences and Environmental Engineering, Southwest Jiaotong University, Chengdu 611756, China
Email: xyzhao2@swjtu.edu.cn

Dr. Nikolaos Nikitas
University of Leeds, School of Civil Engineering, Leeds, LS2, 9JT, UK
Email: N.Nikitas@leeds.ac.uk

* Corresponding author, Email address: yuanran@swjtu.edu.cn

Statements and Declarations

The authors declare that they have no known competing financial interests or personal relationships that could have appeared to influence the work reported in this paper.

Main manuscript

Slope stability analysis considering the strength anisotropy of *c*-*φ* soil

Yi He[a,b], Zhi Li[b], Wenfa Wang[b], Ran Yuan*[a,c], Xiaoyan Zhao[b], Nikolaos Nikitas[d]

[a] Key Laboratory of High-speed Railway Engineering, Ministry of Education, Southwest Jiaotong University, Chengdu 610031, China

[b] Faculty of Geosciences and Environmental Engineering, Southwest Jiaotong University, Chengdu 611756, China

[c] Key Laboratory of Transportation Tunnel Engineering, Southwest Jiaotong University, Chengdu 610031, China

[d] University of Leeds, School of Civil Engineering, Leeds, LS2, 9JT, UK

*Correspondence to Dr. Ran Yuan Email address: yuanran@swjtu.edu.cn

Abstract

In traditional slope stability analyses, soil is usually approximated as isotropic. However, naturally cohesive soil deposits are inherently anisotropic, primarily due to the directional arrangement of soil particles during their deposition process. In this paper, a generalized anisotropic constitutive model for *c*-*φ* soil is introduced to evaluate the influence of varying shear strength on slope stability. In this model, the initial strength anisotropy is defined by the variety of friction angles to the direction of principle stress. This model is utilized by two approaches to estimate the slope stability. Firstly, the upper bound limit analysis solution for slope stability is developed, and the factor of safety of the slopes are studied. Secondly, this model is coupled with the finite element method to get insight of the influence of anisotropy on slope stability. One typic case of slope is studied by numerical analyses. It is found that the slope stability is largely overestimated when the strength anisotropy is ignored, and the overestimation, in terms of safety factors, can reach up to 32.9%. The complex interrelations between degree of anisotropy and evolution of the ensuing safety factor is revealed by a series of parametric study in terms of different degrees of anisotropy.

Keywords: Slope stability, Soil anisotropy, Finite element (FE) analysis, Stability, Safety factor, Soil constitutive laws

1. Introduction

Slope failure has been a major cause of human and material losses, and to this reason it has become a popular subject for considerable, concerted research[1-4]. Although various modelling details play a significant role in slope stability analyses, one of the key aspects is the constitutive modelling employed to describe the mechanical behavior of the soil[5]. A wide gap still exists between research and practice,

because typical simple constitutive models used in every-day engineering are not fully capable of describing the complex mechanical behavior of real geomaterials. As such, deformation and safety factor (F_s) predictions may not meet the accuracy requirements. Although the anisotropic mechanical behavior of natural soils has been discussed widely, in traditional analyses, following an oversimplification rationale, soils are most often regarded as isotropic. To recover prediction accuracy for a number of problems in soil mechanics, slope stability included, the shear anisotropy of soil needs to be explicitly considered for a more faithful replication of the soil medium[6-9].

Strength anisotropies of soils are usually classified into two types, the inherent (initial) and induced ones. The former relates to the influence of soil self-weight and tectonic stresses in the process of natural deposition, which results into directionally varying shear strength[9,10]. The latter stems from the rearrangement of particles and the associated change in the void space distribution under external loads[11]. Generally, in the consolidation direction (usually the vertical), soils exhibit higher shear strength than that in the other directions. This has been demonstrated by the finding that the triaxial compression strength is typically higher than the triaxial extensive strength for the same specimens[12,13]. Researchers intend to describe the strength anisotropy by mathematical approach. Specifically, for c-φ soil, a popular anisotropic failure criterion is the one considering the microstructure tensor as proposed by Pietruszczak and Mroz[11] (P-M). Two strength parameters, i.e., cohesion and friction angle, were assumed to vary within the fabric. Lade[14] proposed a 3D failure criterion for cross anisotropic soils by incorporating the P-M anisotropic conception to the Lade model[15]. This combined criterion was validated by experimental results, and any apparent limitations were discussed. Zhong et al[16] studied the influence of parameters in the P-M anisotropic failure criterion. They demonstrated that when the mean value of microstructure distribution approaches a special range, the value of normalized strength will fluctuate intensely. From then on, the P-M theory was adopted and incorporated with many constitutive models to analyze the mechanical behaviors of anisotropic geomaterials[9,17,18]. It should be noted that the P-M theory is complicated and the relevant parameters are not easy to measured, thus it is not convenient to be applied into the practical engineering.

Strength anisotropy of soils has considerable bearing on the limited dependability of many stability analyses, and the action of slopes accounting for anisotropy is a subject that incentivizes relevant explicit studies. Many attempts have been made in the last decades to study the effect of strength anisotropy on slope stability with respect to undrained conditions. Lo[19] studied through undrained compression tests

specimens with different inclinations to the vertical, whereby the results showed that the influence of anisotropy on the stability is significant for flat slopes but smaller for steep slopes. Based on the Casagrande and Carillo's strength anisotropy concept[20], the slope stability has been studied by Chen[21], and Al-Karni and Al-Shamrani[22], using the limit analysis and limit equilibrium methods respectively. Mutual corroborations between the two different methods can enhance output information. For example, effects of strength anisotropy on the stability number for c-φ soil increase with the decrease in the slope angle, and this effect gets more pronounced while the friction angle of the soil is greater than 10°. Al-Shamrani[22] indicated that the geometry of the slip surface is only slightly affected by the degree of anisotropy in the soil cohesion. To satisfactorily describe the slip surface of an undrained slope, some suggestions proposed that three different laboratory tests, i.e., plane strain compression, plane strain extension, and simple shear test, should be carried out to reflect the loading condition at the different location of the slip surface[23,24]. Su and Liao[25] set to get more accuracy with less test datum for slope stability analyses. They proposed a strength criterion, suitable for plane strain conditions, to analyze the shear strength of undrained clay along the failure surface, where the anisotropic slope stability problem can be reduced to isotropic counterparts as a particular case.

Since the directionally varying cohesion can be measured through in-situ test or laboratory test, this characteristic of soil was discussed broadly in slope stability problems for undrained conditions[26]. However, the effects of the internal friction angle varying with the loading direction for slope stability problems, have not been adequately studied[27,28], despite the fact that such effects have been widely discussed by many researchers for porous media[10,29]. In recent years, the application of hollow cylinder tests makes it possible to measure the variation of friction angle more accurately, and also enable validating theoretical anisotropic models (Fig.1)[10,30]. For natural deposited slopes, the directionally arranged soil particles may cause the strength anisotropy. However, in what extent the varying friction angles will impact the t slope stability has not been fully studied. In addition, for convenience in practice, a simply constitutive model where the strength parameters and the anisotropy index can be easily measured is still needed.

In this paper, a newly proposed general plane-strain, elastic perfectly plastic constitutive model incorporating initial strength anisotropy is reviewed. Hooke's law pertains in the elastic regime. The yield criterion, extended from the classical isotropic Mohr-Coulomb yield criterion, takes the initial strength anisotropy into account. The initial strength anisotropy is considered by the variation of the internal

friction angle with the direction of the principal stresses and an associated flow rule is utilized. The strength anisotropy is defined by two parameters, i.e., n and β, which can be measured through hollow cylinder test. The developed constitutive model is firstly introduced into the limit analysis (LA) method. The stability factor ($\gamma H/c$) of slopes are analyzed based on the kinematic theory within the framework of limit analysis. The effects of anisotropic parameters on the stability factor are evaluated. Further, the slope safety factor (F_s) is studied as well. For the purpose of comparison, the anisotropic yield criterion is applied in conjunction with the finite element method (FEM) where a shear strength reduction approach (SSRA) is used to bring the slopes to the point of failure (limit state). The explicit modified Euler algorithm with stress corrections[31,32] is applied to integrate the elastic-plastic stress strain relationship towards calculating the problem stresses. The failure surface and the F_s obtained by the two methods are compared with each other. The influence of strength anisotropy on critical slip surfaces and F_s of slopes are scrutinized, and the explicit sensitivity of the modelled anisotropic parameters are reviewed by FEM.

2. The anisotropic yield criterion

The anisotropic yield criterion employed was first proposed by Yuan et al[28] to describe the friction angle variation with principal stress orientation. The shape of a resulting yield surface is shown in Fig.1. Conventionally, throughout this paper, negative stress denotes compression. For coherence, a brief introduction of the anisotropic criterion derivation follows.

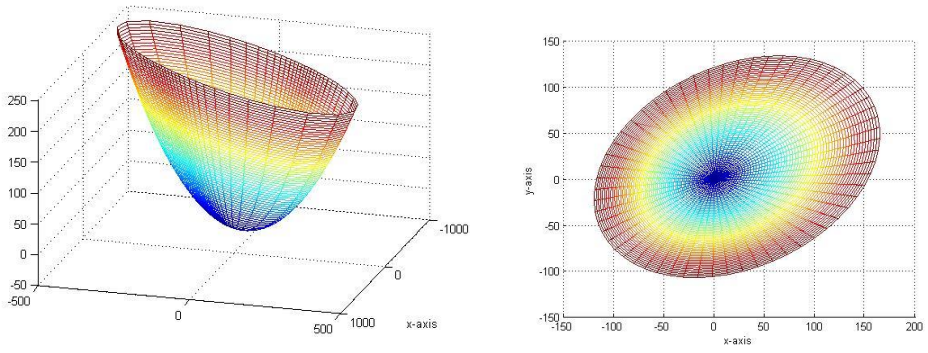

Fig.1 General yield surface: (a) three dimensional stress space [$(\sigma_x+\sigma_y)/2$, $(\sigma_x-\sigma_y)/2$, σ_{xy}], and (b) the cross-section in the stress space of [$(\sigma_x-\sigma_y)/2$, σ_{xy}]

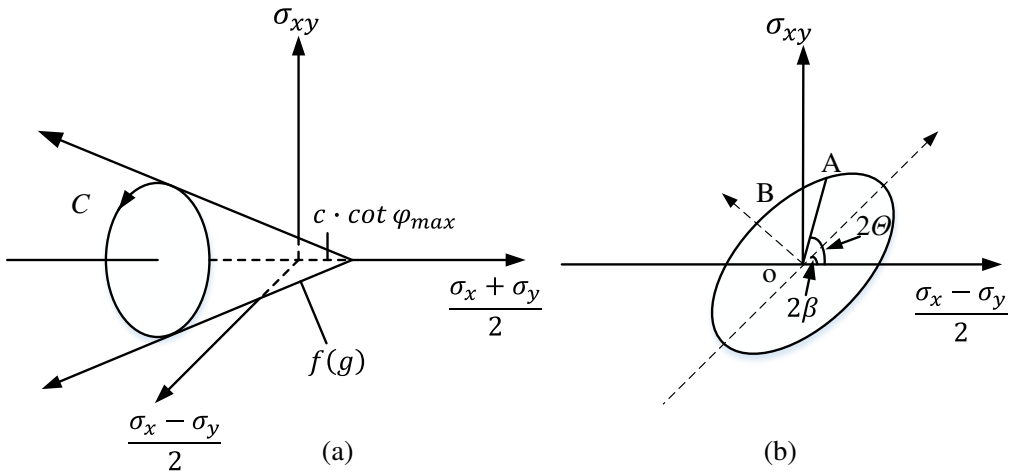

Fig.2 Yield surface in the stress space of (a) three dimension; (b) $(\sigma_x\text{-}\sigma_y)/2$, σ_{xy}

Booker and Davis[33] proposed the hypothesis that the anisotropic yield surface of granular materials can be characterized by the hydrostatic pressure p and the principal stress direction Θ. Yuan et al (2019) as per Booker and Davis (1972), considered the yield surface in the $[(\sigma_x\text{-}\sigma_y)/2,\ \sigma_{xy}]$ space as an ellipse (Fig.2) demonstrating that the anisotropic yield criterion can be explicitly given by

$$f(\sigma_x, \sigma_y, \sigma_{xy}) = R + F(p, \Theta) = 0\,, \tag{1}$$

with

$$R = \frac{1}{2}\sqrt{(\sigma_x - \sigma_y)^2 + 4\sigma_{xy}^2}\,, \tag{1a}$$

$$F(p, \Theta) = (p - c\cot\phi_{\max}) \cdot \sin\phi(\Theta)\,, \tag{1b}$$

$$p = \frac{1}{2}(\sigma_x + \sigma_y)\,, \tag{1c}$$

$$\tan(2\Theta) = \frac{2\sigma_{xy}}{\sigma_x - \sigma_y}\,, \tag{1d}$$

and where, f defines the yield function, R is the distance between the stress point and the origin of coordinates, c is the soil cohesion, φ_{max} is the maximum peak internal friction angle. n and β are the anisotropic parameters, $n=\sin\varphi_{min}/\sin\varphi_{max}$ ranging from 0 to 1, with smaller value denoting more significant anisotropy of soil strength. When n=1, Equation (1) becomes the classical isotropic Mohr-Coulomb yield function. β is the direction angle corresponding to the maximum internal friction angle, namely, when $\Theta=\beta$, $\sin\varphi = \sin\varphi_{max}$. β ranges from 0 to π/4.

Based on the geometry of the ellipse, the variation of friction angles with direction of principal stress can be defined as

$$\sin\phi(\Theta) = \frac{n \cdot \sin\varphi_{\max}}{\sqrt{n^2 \cdot (\cos(2\Theta - 2\beta))^2 + (\sin(2\Theta - 2\beta))^2}} \tag{2}$$

For a specific soil with given c, φ_{max}, n, β, the shear strength parameter sinφ variation with the major length of the ellipse direction Θ, which is shown in Fig. 3, has been previously studied by Yuan et al[10]. This yield criterion has been validated by both experimental and micro-mechanical evidence, and its application to boundary value problems has been showcased[10].

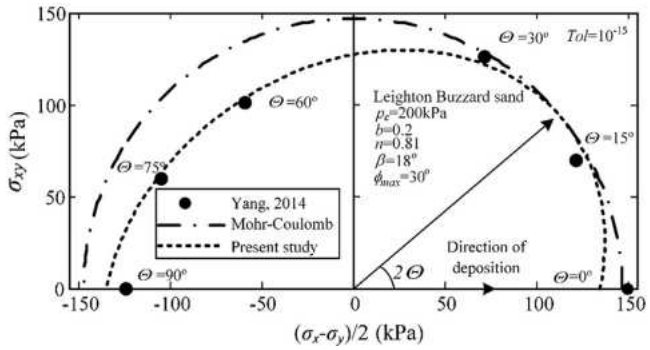

Fig.3 Validation of the newly proposed anisotropic yield criterion[10].

3. Upper bound theory and stability factor

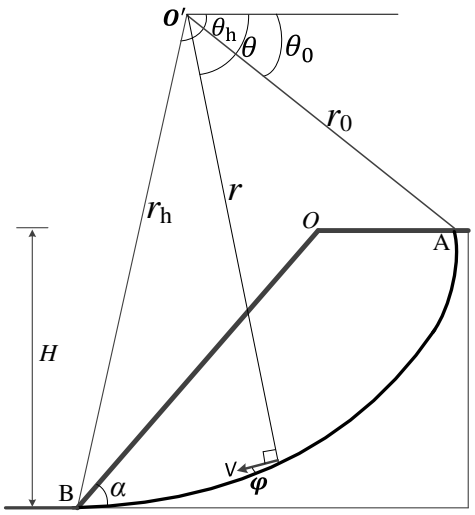

Fig.4. The failure mechanism for a slope.

3.1 LA and stability factor

The compatible velocity field for an upper-bound solution of slope stability is shown in Fig.4. The region AOB rotates as a rigid body about the center of rotation O with the materials below the logarithmic surface AB remaining at rest. The equation for the logarithmic spiral slip surface is given by:

$$r = r_0 \exp[(\theta - \theta_0)\tan\varphi] \quad (3)$$

where r_0 is the length of chord OA, θ_0 is the angle between the chord OA and the horizontal. Note that for an isotropic material, the internal friction angle is constant; however, in this manuscript, the

anisotropic soil is discussed, the value of internal friction angle is dependent on the value of Θ, β, and n, and it can be calculated by Eq.(2). The rate of external work for the region ABO is calculated by the algebraic summation:

$$\dot{W} = \gamma r_0^3 \omega (f_1 - f_2 - f_3) \tag{4}$$

where γ is the soil weight, ω is the rotational angular velocity of the block ABO, f_1-f_3 are the coefficients for the calculation of the soil weight work rate, which can be found in the literature[21].

The internal dissipation of energy occurs along the slip surface AB. The total internal dissipation energy is obtained by the following integration:

$$D = \int_{\theta_0}^{\theta_h} c(V\cos\varphi)\frac{rd\theta}{\cos\varphi} = \frac{cr_0^2\omega}{2\tan\varphi}\left\{\exp[2(\theta_h - \theta_0)\tan\varphi] - 1\right\} \tag{5}$$

Equating the external rate of work to the internal energy dissipation rate, yields:

$$H = \frac{c}{\gamma}F(\theta_h, \theta_0) \tag{6}$$

where the function $F(\theta_h, \theta_0)$ can be calculated as:

$$F(\theta_h, \theta_0) = \frac{\sin\beta\left\{\exp[2(\theta_h - \theta_0)\tan\varphi] - 1\right\}}{2\sin(\beta - \alpha)\tan\varphi(f_1 - f_2 - f_3)}\left\{\sin\theta_h \exp[(\theta_h - \theta_0)\tan\varphi] - \sin\theta_0\right\} \tag{7}$$

Apparently, $F(\theta_h, \theta_0)$ is a function of parameters θ_h and θ_0, and its minimum value can be calculated using optimization approach. Based on Eq.(6), the least upper bound of the critical height H_c is obtained when the minimum value of $F(\theta_h, \theta_0)$ is obtained. Denoting $N_s = \min F(\theta_h, \theta_0)$, associating with Eq.(6), we have:

$$N_s = \frac{\gamma H_c}{c} = \min F(\theta_h, \theta_0) \tag{8}$$

N_s is a dimensionless number, also known as the stability factor of the slope. For a slope with specific isotropic strength parameters, the value of N_s depends on the slope angle α and the internal friction angle φ. In this case, the stability factor is also affected by the anisotropic coefficients n and β. The coefficient Θ is assumed to be 70° in the kinematic approach of limit analysis. The parametric study of the anisotropic coefficients on the stability factor of the slope is carried out in the following. Fig. 5(a) shows that the decreasing value of parameter n results in the decrease in the stability factor. For a specific value of n, the stability factor decreases with the increasing parameter β until β approaches 25°, where the

stability factor reaches the minimum value. Thereafter the stability factor increases gradually with the increasing parameter β. Note that when n=1, the stability factor is constant even the parameter β varies from 0 to 45°, because n=1 denotes the isotropic condition. Not surprise, the stability factor increases with the increasing maximum internal friction angle φ_{max} no matter the anisotropic condition is considered or not (Fig.5b). Note that the differences between the results from the isotropic and that of anisotropic become pronounced with the increase in φ_{max}.

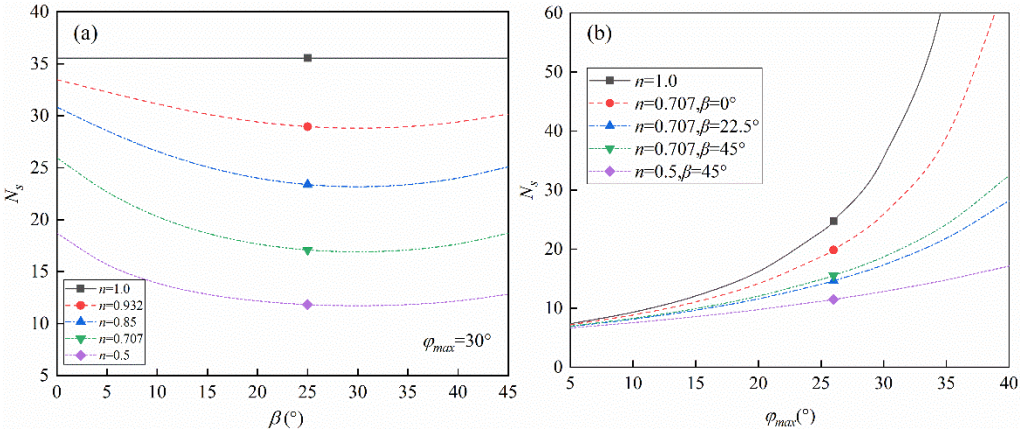

Fig.5. The effects of anisotropic parameters on stability factor (slope angle α=45°).

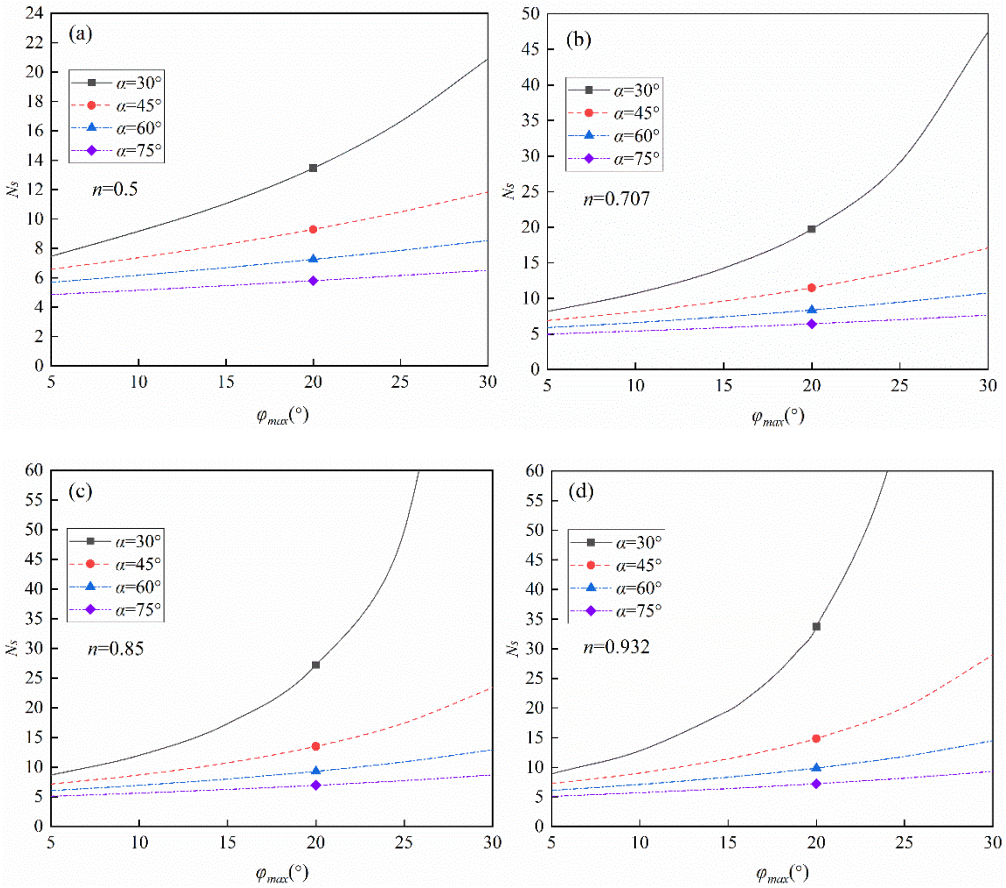

Fig. 6. The effect of slope angle α on the stability factor (β=25°): (a) n=0.5, (b) n=0.707, (c) n=0.85,

(d) n=0.932.

When the anisotropic parameter β=25°, the stability factor varies with the maximum internal friction angle φ_{max} for different slope angles are shown in Fig.6. The increasing parameter n has significant effect on the stability factor for gentle slopes ($\alpha \leq 45°$), while a less obvious effect is observed in steep slopes ($\alpha \geq 60°$). For instance, when φ_{max}=15°and n=0.5, the stability factor for the slopes with the inclination angle of 30° and 75° are 11.04, 5.46, respectively. Whereas, the counterpart is 19.51 and 6.40 when n=0.932. The growth rate is 77% and 17% for the gentle and steep slopes, respectively.

3.2 The SSRA and safety factor

Based on the SSRA, the safety factor can be defined as:

$$c' = c / F_s \tag{9}$$

$$\tan\varphi' = \tan\varphi / F_s \tag{10}$$

where c'and φ' are the soil strength parameters necessary only to maintain the structure in limit equilibrium and sometimes referred to as the mobilized strength parameters.

Factored shear strength parameters c', φ' are used to bring the slope to the point of failure. Substituting Eqs.(2),(9), and (10) into Eq.(6), the safety factor can be calculated. To avoid the iteration, the stability charts are presented herein for slopes with specific $\gamma H/c$, α, β, and n in the following.

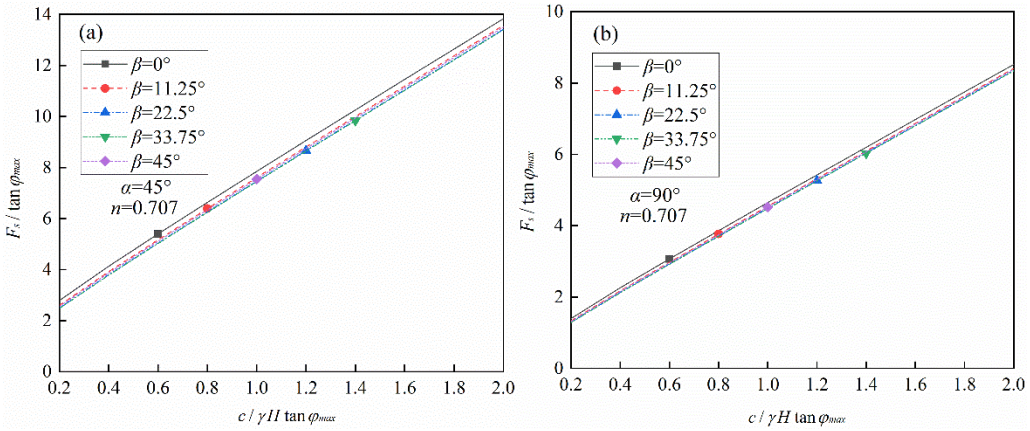

Fig.7. Stability chart for slopes considering strength anisotropy: (a) α=45°, (b) α=90°

In order to make a quick estimate of the slope stability considering soil strength anisotropy, the stability chart is presented in Fig.7. For a specific slope, the maximum value of F_s can be obtained with β=0°. In addition, it is shown that for a specific slope with known values of $c/(\gamma H\tan\varphi_{max})$ and slope angles α, the factor of safety of slope can be obtained from Fig.7 without any iteration. For example, a slope inclined at 45°, with the height of 10m, the soil unit weight is 18kN/m^3, the soil cohesion is 22kPa,

the maximum internal friction angle φ_{max}=17°, the anisotropic parameters are tested by lab test (n=0.707, β=11.25°). It can be calculated that $c/(\gamma H\tan\varphi_{max})$=0.4. We can get that $F_s/\tan\varphi_{max}$=3.928 from the red line in Fig.7a. Then, the factor of safety is calculated as F_s=1.2.

4. The numerical analysis procedure

It has been widely accepted that the slope stability is significantly affected by strength anisotropy of soils[18,21]. To this purpose, a comparison between the influences of isotropic and anisotropic strength on slip surface of slopes is sought. The SSRA associated with FEM was proposed by Zienkiewicz et al [34], and a good agreement with the slip circle solution was obtained for c-φ soil slopes. This approach was extended by many to slope stability analysis[35-38], and is adopted here, with a summary of the procedure presented in what follows. The definition of safety factor is the same with reference to Eqs.(9) and (10). An iteration process is required to establish the expression of F_s. When the slope failure occurs, the factor F_s is the desired solution.

The slope stability analysis inherently refers to an elastoplastic problem. The quadrilateral isoparametric element is used for modelling in FEM. In the elastic regime, the Hooke's law is considered, while in the plastic regime, the stress-strain relationship in its incremental form is given as:

$$\dot{\boldsymbol{\sigma}} = \Delta\boldsymbol{\sigma}_e - \Delta\lambda \boldsymbol{D}(\partial g/\partial\boldsymbol{\sigma}) \tag{12}$$

where $\Delta\boldsymbol{\sigma}_e$ stands for the vector of elastic stresses, $\Delta\boldsymbol{\sigma}_e=\boldsymbol{D}\Delta\boldsymbol{\varepsilon}$ ($\Delta\varepsilon$ is the strain rate); D is the stress-strain matrix; g is the plastic potential; and $\Delta\boldsymbol{\lambda}$ can be calculated as

$$\Delta\boldsymbol{\lambda} = \frac{\boldsymbol{D}(\partial f/\partial\boldsymbol{\sigma})^T \Delta\boldsymbol{\varepsilon}}{(\partial f/\partial\boldsymbol{\sigma})^T \boldsymbol{D}(\partial g/\partial\boldsymbol{\sigma})} \tag{13}$$

in which, f is the yield function. When the associated flow rule is applied, the expression of plastic potential g equals to that of the yield function f.

After the initial yielding is determined, the explicit modified Euler integration scheme with stress correction[32] is applied to calculate the elastoplastic stress and strain. Strain hardening is not considered, and all the stresses and strains are integrated at the Gauss points. The Newton-Raphson method has been found to converge rapidly in FE codes. The displacement mutation of the characteristic point combining with the continuums of the plastic zone can be regarded as a reliable definition of slope failure. The procedure of the iteration algorithm used can be found in the literature[38]. The implementation of the proposed yield function into FE analysis faces computational challenges, mainly because of the gradient

239 discontinuities at the tip or vertex of the yield surface. This particular issue can be tackled by a number
240 of methods aiming to remove singularities in the yield surface. Among these, the method proposed by
241 Abbo and Sloan[39] is adopted by introducing a parameter a=0.05$c$cotφ_{max}. This latter so called hyperbolic
242 approach can be found for brevity in the appendix.
243

244 **5. Case study**

245 One numerical examples of typical soil slope models are used to analyze the effects of strength
246 anisotropy on slope stability. The geometry of the slopes and the material properties of the soils are
247 adopted as in Dawson[40]. Parametric studies on the influence of degree of the strength anisotropy, in
248 terms of anisotropic parameters, on the slope stability problem are presented. Anisotropic parameters are
249 following Yuan et al[10].

250 A simple slope adopted from Dawson[40] is shown in Fig.8. The slope has a height of 10m with a
251 base of 3m, and the inclination of the slope is 45°. The four-node quadrilateral isotropic element is
252 utilized to discretize the slope model, with a total number of 330 elements and 369 nodes. On the left and
253 right boundaries, vertical rollers are applied to restrict the horizontal displacement, while full fixity is
254 applied at the base. The properties of the soil are listed in Table 1. It has been discussed by Griffith and
255 Lane[35] that the values of Young's modulus and Poisson's ratio have negligible influences on the
256 predicted F_s. Typical values are given to the soils, namely, E=10000kN/m^2, υ=0.3. The selection for the
257 anisotropic parameters n and β will be detailed in what follows. The associated normality flow rule for
258 elastoplastic material is used. As mentioned above, the displacement mutation of the characteristic point
259 (point a in Fig.8) combing with the continuums of the plastic zone from the slope toe to top is regarded
260 as the nominal slope failure condition.

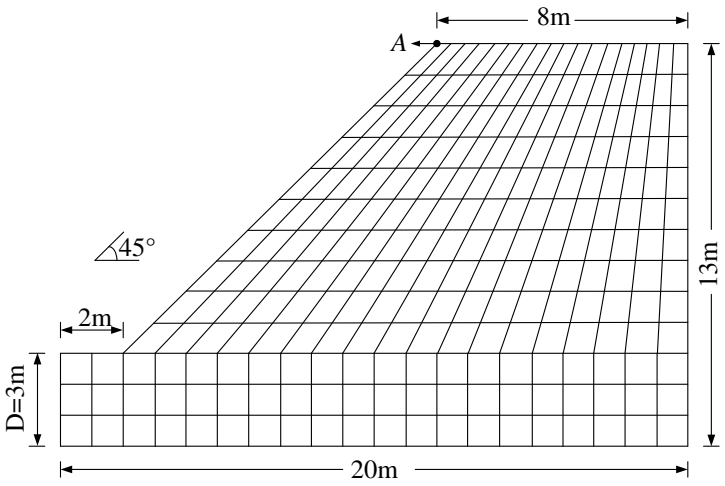

Fig.8. The discrete mesh of soil slope model.

Table 1. Material properties.

Unit weight γ (kN/m^3)	Friction angle φ_{max} (°)	Dilation angle ψ (°)	Cohesion c (kPa)
20	20	20	12.38

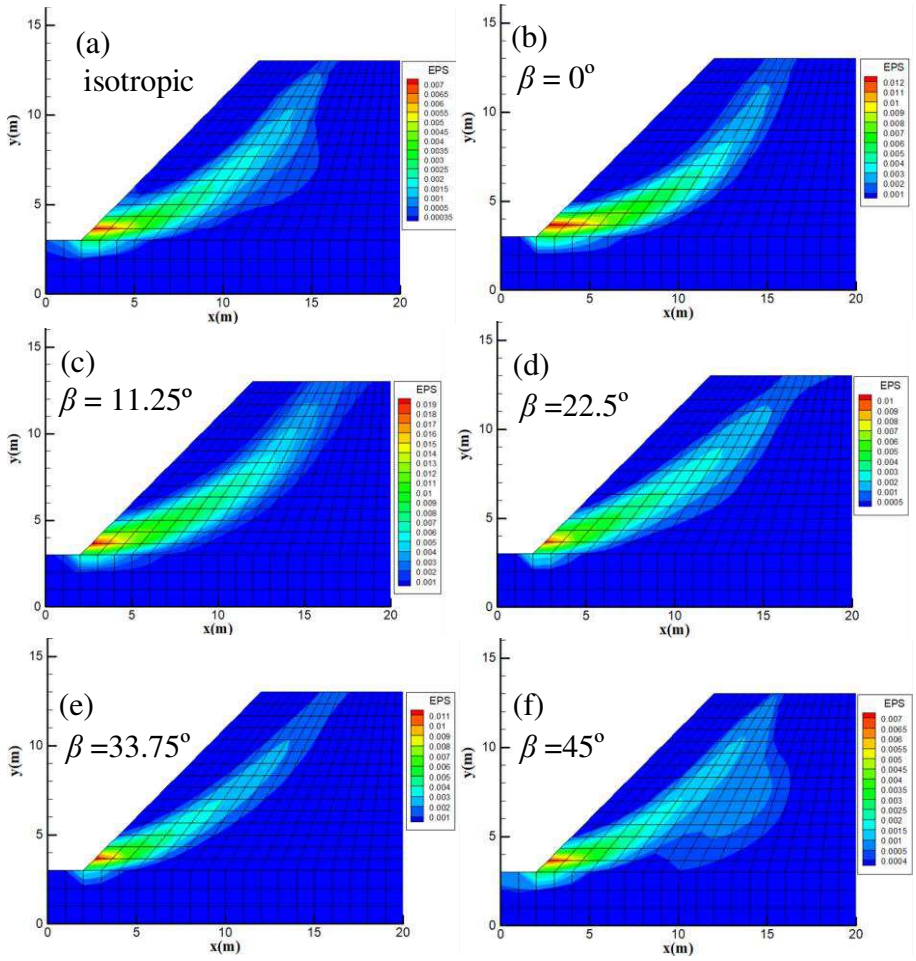

Fig.9. Equivalent plastic strain nephograms of slopes for isotropic and anisotropic [(b)~(f), n=0.707] conditions: (a) isotropic(n=1), F_s=1.03; (b) F_s=0.89; (c) F_s=0.825; (d) F_s=0.79; (e) F_s=0.81; (f) F_s=0.87.

The equivalent plastic strain (EPS) nephograms of the slope for isotropic and anisotropic conditions are displayed in Fig.9. It has been previously calculated that the F_s of this slope is exactly 1.0 for homogeneous isotropic condition through limit analysis[21]. Dawson et al[40] worked out the F_s and estimated it to be between 1.02 and 1.03, by using FEM combined with SSRA. It has been demonstrated that the numerical results are a little different than the limit analysis solutions for most of the times, but within reasonable bounds. In this paper, the calculated F_s of the isotropic slope is 1.03, which well agrees with the literature. Figs.4 (b)~(f) show the anisotropic results. It is depicted that when n =0.707, the F_s is always lower than 1.0. The trace of EPS, which can be regarded as the slip surface, varies with the value of anisotropic parameter β. With increasing β, the slip surface is gradually moving away from the slope shoulder until approximately β=22.5°, after which it starts returning closer to the shoulder. Fig.9 demonstrates that the consideration of strength anisotropy will lead to a more critical failure mechanism.

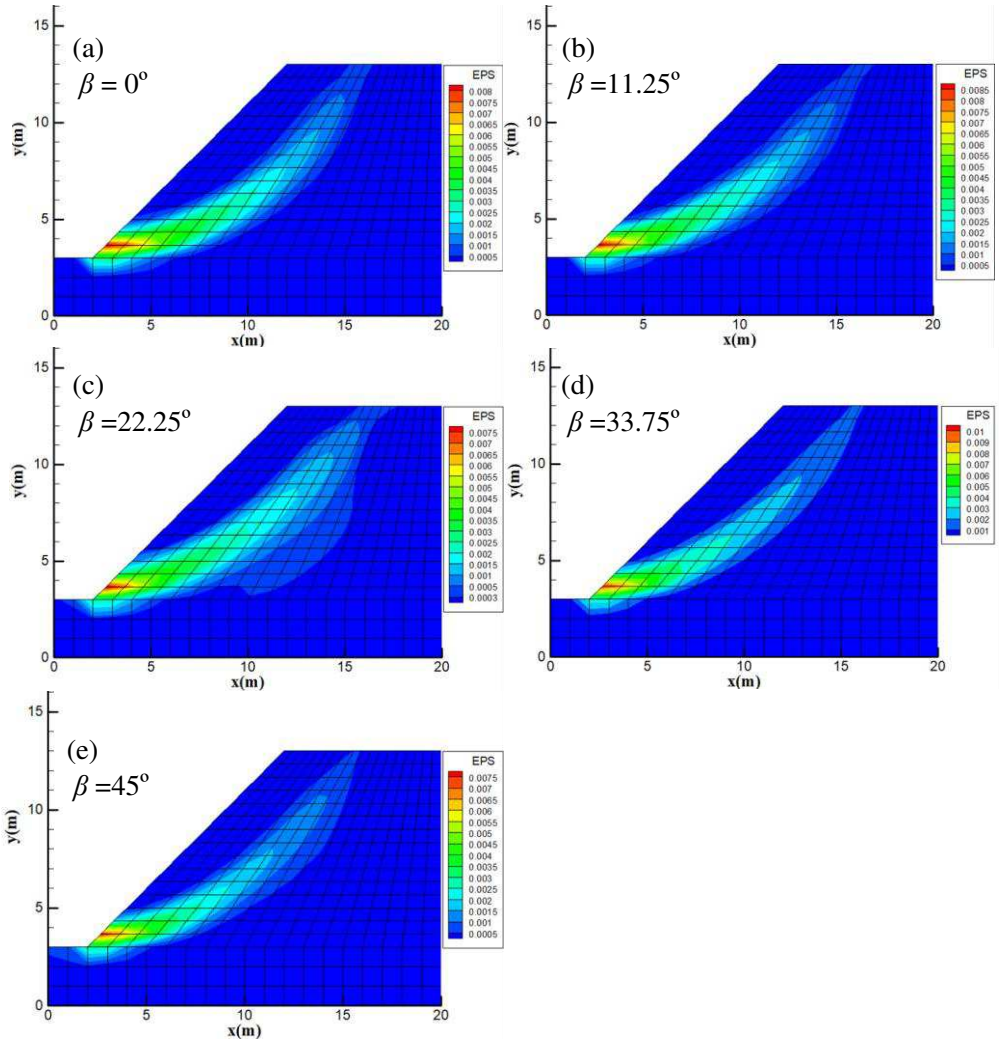

Fig.10. Equivalent plastic strain nephograms of slopes for anisotropic conditions(n=0.85): (a) F_s=0.97; (b) F_s=0.94; (c) F_s=0.92; (d) F_s=0.94; (e) F_s=0.96.

When the parameter n=0.85, the EPS nephograms are displayed in Fig.10. The strength anisotropy results again in a lower F_s than in those from the isotropic solution. The F_s in Fig.10 are all very close to the isotropic solution, i.e., 1.03, with the β values varying equidistantly from 0° to 45°. In addition, comparing with Fig.9, there is not much difference relevant to the shape of the slip surface for different β values. It is because the n value in Fig.10 is larger than that in Fig.9. As mentioned before, the closer to 1 the n value, the anisotropic effect diminishes. The F_s of slopes for different β values are collected in Fig.11. It is shown that for a specific value of n, the F_s of slopes decreases with the increase in β until β=22.5°, for the actual β sampling considered. There the F_s reaches a nominal minimum value, and then increases gradually for even higher β. Fig.11 also displays that for a given β value, a smaller n value results in a lower F_s. This is because the n value defines the shape of the anisotropic yield surface, which is an ellipse. The larger the n value, the shape of the yield surface is more approaching a circle, namely, and the soil performs closer to the less onerous isotropic condition. Generally, if the strength anisotropy is neglected, the overestimation of F_s can get up to 32.9% for n=0.707; and 14.1% for when n =0.85.

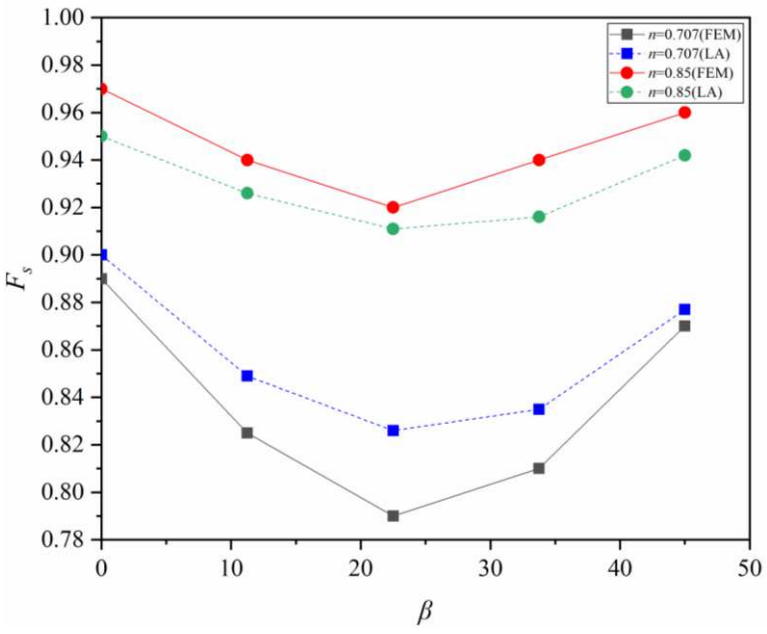

Fig. 11. Factor of safety of slopes against the anisotropic parameter β.

6. Conclusions

Soils, although having their anisotropic mechanical performance recognized, they are mostly regarded as isotropic in traditional slope stability analyses. This deficiency may result in the

overestimation of factors of safety. To this reason, slope stability analyses considering the strength anisotropy have been recently carried out in order to seize explicit anisotropy effects. However, most of them focus on undrained soils. In this paper, an anisotropic yield criterion was introduced to analyze the influence of strength anisotropy on generic *c*-φ soil type slopes.

The anisotropic yield criterion was combined with kinematic method of limit analysis and FEM respectively to analyze the slope stability. The stability charts were presented to make a quick estimation of the F_s. The values of F_s obtained by LA and FEM showed highly agreement one another. The slope stability was largely overestimated if the strength anisotropy was ignored. For instance, the maximum overestimation can reach up to 32.9% for the presented case. The parametric analysis shows that the increasing parameter *n* resulted in a pronounced increasement in the stability factor for steep slopes ($\alpha \geq 60°$), whereas, this increasement was less sensitive for gentle slopes ($\alpha \leq 45°$). In addition, the presented case showed that for a given *n* value, a minimum peak factor of safety was obtained when β=22.5°

Appendix

In displacement-based FE analysis, the traditional Mohr-Coulomb yield function presents a number of computational difficulties due to the gradient discontinuities which occur at the tip of the yield surface and the edges of the hexagonal yield surface pyramid. To avoid these computational difficulties, a number of methods have been proposed to remove the associated gradient singularities. In the present paper, the method proposed by Abbo and Sloan[39] has been adopted, and this is briefly described below.

A hyperbolic approximation in the meridional plane is used to eliminate the tip singularity. In (σ_m, $\bar{\sigma}$) space, the hyperbolic approximation to the Mohr-Coulomb yield criterion is shown in Fig. A1

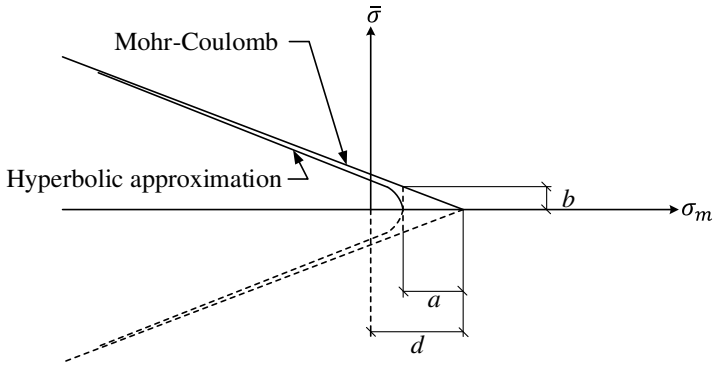

Fig. A1 Hyperbolic approximation to Mohr-Coulomb yield criterion[32].

The equation of the hyperbola in Fig.A1 can be mathematically described by:

$$f = \sigma_m + \sqrt{J_2 K^2(\theta) + \alpha^2 \sin^2\varphi} - c\cos\varphi = 0 \tag{A1}$$

in which,

$$\sigma_m = \frac{1}{3}(\sigma_x + \sigma_y + \sigma_z) \tag{A2}$$

$$J_2 = \frac{1}{2}(s_x^2 + s_y^2 + s_z^2) + \tau_{xy}^2 + \tau_{yz}^2 + \tau_{xz}^2 \tag{A3}$$

$$\begin{aligned} K(\theta) &= A - B\sin 3\theta \quad (|\theta| > \theta_T) \\ K(\theta) &= \cos\theta - \frac{1}{\sqrt{3}}\sin\varphi\sin\theta \quad (|\theta| \le \theta_T) \end{aligned} \tag{A4}$$

$$\begin{aligned} A &= \frac{1}{3}\cos\theta_T[3 + \tan\theta_T \tan 3\theta_T + \frac{1}{\sqrt{3}} sign(\theta)(\tan 3\theta_T - \tan\theta_T)\sin\varphi] \\ B &= \frac{1}{3\cos 3\theta_T}(sign(\theta)\sin\theta_T + \frac{1}{\sqrt{3}}\sin\varphi\cos\theta_T) \end{aligned} \tag{A5}$$

$$\begin{aligned} sign(\theta) &= +1 \quad (\theta \ge 0^\circ) \\ sign(\theta) &= -1 \quad (\theta < 0^\circ) \end{aligned} \tag{A6}$$

We have used Eq.(A1) to model the Mohr-Coulomb yield function. Apparently in Fig.A1, *a* is the distance of the Mohr-Coulomb yield surface tip and the hyperbola tip, and a smaller value of *a* represents a closer approximation of the Mohr-Coulomb yield surface. The hyperbolic yield surface with various *a* values is displayed in Fig. A2.

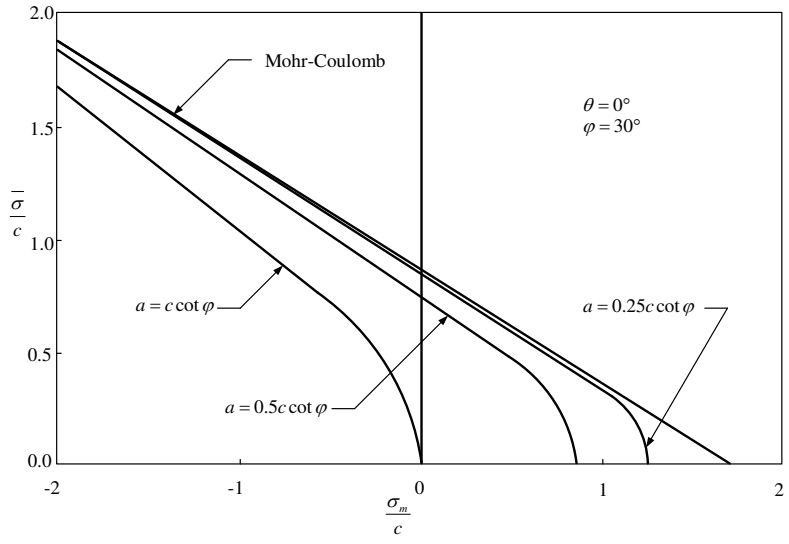

Fig. A2 Hyperbolic approximation to Mohr-Coulomb meridional section[32].

More details of the hyperbolic yield surface can be found in Abbo[32] and He et al[38].

Acknowledgments

This work was supported by the National Natural Science Foundation of China (Grant Nos. 42077236, 42011530170), Sichuan Science and Technology Program (Grant No. 2021YFH0031, 2021YFS0320), Guangxi State Key Laboratory of Disaster Prevention, Mitigation and Engineering safety (Grant No.2019ZDK046), and by Royal Society grant (IEC\NSFC\191675 - International Exchanges 2019 Cost Share (NSFC)). These supports are gratefully acknowledged.

Data availability

Some or all data, models that support the findings of this study are available from the corresponding author upon reasonable request.

Author contributions

Yi He: Conceptualization, Methodology, Writing-original draft, Writing-review & editing. **Zhi Li**: Software, Formal analysis, Visualization, Writing-original draft. **Wenfa Wang**: Software, Formal analysis, Writing-review & editing. **Ran Yuan**: Conceptualization, Supervision, Funding acquisition, Project administration, Writing-review & editing. **Xiaoyan Zhao**: Methodology, Software. **Nikolaos Nikitas**: Methodology, Writing-review & editing, Funding acquisition. All authors have read and agreed the published version of the manuscript.

Competing interests

The authors declare they have no financial interests.

References

[1] Ugai, K. A method of calculation of total safety factor of slope by elasto-plastic FEM. *Soils and Foundations* **29,** 190–195 (1989).

[2] Yu, H. S., Salgado, R., Sloan, S.W., Kim JM Limit analysis versus limit equilibrium for slope stability. *Journal of Geotechnical and Geoenvironmental Engineering* **124,** 1-11 (1998).

[3] He, Y., Liu, Y., Zhang, Y. B., Yuan, R. Stability Assessment of Three-Dimensional slopes with Cracks. *Engineering Geology* **252,** 136-144 (2019).

[4] Zhao, L. H., Zuo, S., Lin, Y. L., Li, L., Zhang, Y. B. Reliability back analysis of shear strength parameters of landslide with three-dimensional upper bound limit analysis theory. *Landslides* **13,** 711–724 (2016).

[5] Schweiger, H.F., Wiltafsky, C., Scharinger, F., Galavi, V. A. multilaminate framework for modelling induced and inherent anisotropy of soils. *Geotechnique* **59,** 87-101 (2009).

[6] Takaharu, S., Naohisa, K. A slope stability analysis of considering undrained strength anisotropy of natural clay deposits. *Soils and Foundations* **48,** 805-819 (2008).

[7] Loukidis, D., Salgado, R. Effect of relative density and stress level on the bearing capacity of footings on sand. *Geotechnique* **61,** 107-119 (2011).
[8] Gonzalaz, N. A., Rounainia, M., Arroyoi, M., Gens, A. Analysis of tunnel excavation in London clay incorporating soil structure. *Geotechnique* **62,** 1095-1109 (2012).
[9] Yao, Y., Tian, Y., Gao, Z. Anisotropic UH model for soils based on a simple transformed stress method. *International Journal for Numerical and Analytical Method in Geomechanics* **41,** 54-78 (2017).
[10] Yuan, R., Yu, H. S., Yi, H., He, Y. Non-coaxial soil model with an anisotropic yield criterion and its application to the analysis of trip footing problems. *Computers and Geotechnics* **99**, 80-92 (2018).
[11] Pietruszczak, S., Oboudi, M. Description of induced anisotropy in microstructure of granular soils. *Soils and Foundations* **57,** 514-526 (2017).
[12] Bjerrum, L. Problems of soil mechanics and construction on soft clay. *Proceedings 8th International Conference in Soil Mechanics and Foundation Engineering* **3,** 161-190 (1973).
[13] Vaid, Y. P., Sivathayalan, S. Static and cyclic liquefaction potential of Fraser Delta sand in simple shear and triaxial tests. *Canadian Geotechnical Journal* **33,** 281–289 (1996).
[14] Lade, P. V. Modeling failure in cross-anisotropic frictional material. *International Journal of Solids and Structures* **44,** 5146-5162 (2007).
[15] Lade, P. V. Elasto-plastic stress-strain theory for cohesionless soil with curved yield surface. *International Journal of Solids and Structures* **13,** 1019-1035 (1997).
[16] Zhong, S. Y., Xu, W. H., Ling, D. S. Influence of the parameters in the Pietruszczak—Mroz anisotropic failure criterion. *International Journal of Rock Mechanics and Mining Sciences* **48,** 1034-1037(2011).
[17] Gao, Z. W., Zhao, J. D. Efficient approach to characterize strength anisotropy in soil. *Journal of Engineering Mechanics* **138,** 1447-1456 (2012).
[18] Tang, H. X., Wei, W. C., Liu, F., Chen, G. Q. Elastoplastic cosserat continuum model considering strength anisotropy and its application to the analysis of slope stability. *Computers and Geotechnics* **117,** 103235 (2020).
[19] Prevost, J. H. Undrained shear test on clays. *Journal of geotechnical engineering division, American Society of Civil Engineers* **105,** 49-64 (1979).
[20] Casagrande, A., Carillo, N. Shear failure of anisotropic soils. *Journal of Boston Society of Civil Engineering* **31,** (1944).
[21] Chen, W. F., Snitbhan, N., Fang, H. Y. Stability of slopes in anisotropic nonhomogeneous soils. *Canadian Geotechnical Journal* **12,** 145-151 (1975).
[22] Al-Karni, A. A., Al-Shamrani, M. A. Study of the effect of soil anisotropy on slope stability using method of slices. *Computers and Geotechnics* **26,** 83-103 (2000).
[23] Ladd, C. C., Foott, R. New design procedure for stability of soft clay. *Journal of Geotechnical Engineering Division* **100,** 763-786 (1974).
[24] Koutsoftas, D. C., Ladd, C. C. Design strengths for an offshore clay. *Journal of Geotechnical Engineering* **111,** 337-355 (1985).
[25] Su, S. F., Liao, H. J. Effect of strength anisotropy on undrained slope stability in clay. *Geothecnique* **49,** 215-230 (1999).
[26] Kim, J., Salgado, R., Yu, H. S. Limit Analysis of Soil Slopes Subjected to Pore-Water Pressures. *Journal of Geotechnical and Geoenvironmental Engineering* **125,** 49-58 (1999).
[27] Chang, J. F., Chu, X. H., Xu, Y. J. Finite-element analysis of failure in transversely isotrop-ic geomaterials. *International Journal of Geomechanics* **15,** 1-14 (2015).
[28] Yuan, R., Yu, H. S., Yang, D. S., Hu, N. On a fabric evolution law incorporating the effe-cts of b-value.

Computers and Geotechnics **105,** 142–154 (2019).
[29] Oda, M., A mechanical and statistical model of granular material. *Soils and Foundations* **14,** 13-27 (1974).
[30] Yang, D. S. Microscopic study of granular material behavior under general stress paths. *Dissertation, University of Nottingham* (2014).
[31] Sloan, S. W. Substepping schemes for the numerical integration of elastoplastic stress-strain relations. *International Journal for Numerical Methods in Engineering* **24,** 893–911 (1987).
[32] Abbo, A. J. Finite element algorithms for elastoplasticity and consolidation. *Dissertation, University of Newcastle, Callaghan, Australia* (1997).
[33] Booker, J. R., Davis, E. H. A general treatment of plastic anisotropy under conditions of plane strain. *Journal of the Mechanics and Physics of Solids* **20,** 239–250 (1972).
[34] Zienkiewicz, O. C., Humpheson, C., Lewis, R. W. Associated and non-associated visco-plasticity and plasticity in soil mechanics. *Geotechnique* **25,** 671–689 (1975).
[35] Griffiths, D. V., Lane, P. A. Slope stability analysis by finite elements. *Geotechnique* **49,** 387-403 (1999).
[36] Sloan, S. W. Geotechnical Stability Analysis. *Geotechnique* **63,** 531-571 (2013).
[37] Smith, I. M., Griffiths, D. V., Margetts, L. Programming the finite element method. *John Wiley & Sons 5th Edition* (2014).
[38] He, Y., Wang, X. Y., Yuan, R., Liu, K. W., Zhuang, P. Z. On the Computational Precision of Finite Element Algorithms in Slope Stability Problems. *Mathematical Problems in Engineering* **4,** 1-15 (2019).
[39] Abbo, A. J., Sloan, S. W. A smooth hyperbolic approximation to the Mohr-Coulomb yield criterion. *Computers & Structures* **54,** 427–441 (1995).
[40] Dawson, E. M., Roth, W. H., Drescher, A. Slope stability analysis by strength reduction. *Geotechnique* **49,** 835–840 (1999).

Supplementary Files

This is a list of supplementary files associated with this preprint. Click to download.

- SupplementaryMaterial.docx